Ceramics International xxx (xxxx) xxx–xxx

Contents lists available at ScienceDirect

Ceramics International

journal homepage: www.elsevier.com/locate/ceramint

Structure and microwave dielectric properties of $SrLa[Al_{1-x}(Mg_{0.5}Ti_{0.5})_x]O_4$ (x = 0.2–0.8) ceramics

Gu Yi Chen[1], Guang Rong Ren[1], Lei Li*, Bing Liu, Xiang Ming Chen

Laboratory of Dielectric Materials, School of Materials Science & Engineering, Zhejiang University, Hangzhou 310027, China

ARTICLE INFO

Keywords:
Microwave dielectric properties
K_2NiF_4–type structure

ABSTRACT

Dense $SrLa[Al_{1-x}(Mg_{0.5}Ti_{0.5})_x]O_4$ (x = 0.2–0.8) ceramics were prepared by a standard solid state sintering method. The K_2NiF_4–type layered perovskite structure with *I4/mmm* space group was revealed by XRD over the whole composition range, indicating that $SrLaAlO_4$ and $SrLa(Mg_{0.5}Ti_{0.5})O_4$ can form infinite solid solution. The evaluation of the refined structure was investigated by Rietveld analysis of XRD and Raman spectrum. The dielectric constant (ε_r) and temperature coefficient of resonant frequency (τ_f) increased with increasing x, while the *Qf* value first increased and then decreased. The measured ε_r was significantly lower than the predicted value from Clausius-Mosotti relationship, and their difference approached 0 with increasing x, which is mainly attributed to the increasing normalized bond lengths of Sr/La-O(1) and Sr/La-O(2a) bonds. The optimal microwave dielectric properties with ε_r = 22.2, *Qf* = 89,100 GHz and τ_f = −0.1 ppm/°C were obtained for x = 0.65, indicating that $SrLa[Al_{1-x}(Mg_{0.5}Ti_{0.5})_x]O_4$ solid solution is a promising candidate as low-loss microwave dielectric ceramics.

1. Introduction

In the recent years, *MLn*AlO_4-based microwave dielectric ceramics (*M* = Sr and Ca, *Ln* = La, Nd, Sm, and Y) have attracted continuous attention due to the ultra-low dielectric loss [1,2]. *MLn*AlO_4 ceramics are of tetragonal K_2NiF_4–type layered perovskite structure with *I4/mmm* space group, and the temperature coefficient of resonant frequency (τ_f) is usually a negative value [1,2]. The near-zero τ_f has been obtained in their solid solutions with M_2TiO_4, together with a dielectric constant (ε_r) around 20 and a high *Qf* value varying from 75,000 to 100,000 GHz [3–6]. Comparing with the typical competitors $MgTiO_3$-$CaTiO_3$ composites [7] and noble element-containing complex perovskites such as $Ba(Mg_{1/3}Ta_{2/3})O_3$ and $Ba(Zn_{1/3}Ta_{2/3})O_3$ [8], good combination of high *Qf* value and low cost can be achieved in *MLn*AlO_4-based ceramics with near-zero τ_f.

The structure of *MLn*AlO_4 can be regarded as the interpenetrating stacking of a perovskite layer (*M*, *Ln*)AlO_3 and a rock-salt layer (*M*, *Ln*)O along *c* axis, and the perovskite layer is tightly related with the *Ln*AlO_3 simple perovskite [9]. Al^{3+} in *Ln*AlO_3 simple perovskite can be replaced by aliovalent cations $(R_{0.5}Ti_{0.5})^{3+}$ (*R* = Mg, Zn), so that the simple perovskite converts to a complex perovskite [10,11]. Similarly, Al^{3+} in *MLn*AlO_4 may also be replaced by $(R_{0.5}Ti_{0.5})^{3+}$. For example, single-phase $SrLa(Mg_{0.5}Ti_{0.5})O_4$ and $SrLa(Zn_{0.5}Ti_{0.5})O_4$ ceramics with K_2NiF_4–type structure and *I4/mmm* space group have been prepared, and their microwave dielectric properties are as following: ε_r = 25.5, *Qf* = 72,000 GHz, τ_f = 29 ppm/°C for $SrLa(Mg_{0.5}Ti_{0.5})O_4$, and ε_r = 29.4, *Qf* = 34,000 GHz, τ_f = 38 ppm/°C for $SrLa(Zn_{0.5}Ti_{0.5})O_4$ [12]. Different from the analogue $SrLaAlO_4$ ceramic with a large negative τ_f value of −32 ppm/°C [3], $SrLa(R_{0.5}Ti_{0.5})O_4$ ceramics are of positive τ_f values, and the nero-zero τ_f is expected in $SrLaAlO_4$-$SrLa(R_{0.5}Ti_{0.5})O_4$ solid solutions. Furthermore, it has been deduced that $SrLaAlO_4$ and $SrLa(R_{0.5}Ti_{0.5})O_4$ can form unlimited solid solution according to the discussion on the stability of K_2NiF_4–type structure in *MLnB*O_4 (M = Ca, Sr, Ba; Ln = Y, Sm, Nd, La; *B* = Al, Ga, $(Mg_{0.5}Ti_{0.5})$, $(Zn_{0.5}Ti_{0.5})$) compounds in relation to the tolerance factor of perovskite layer and the radius ratio of M^{2+} and Ln^{3+} [12]. In fact, this has been proven in $SrLaAlO_4$-$SrLa(Zn_{0.5}Ti_{0.5})O_4$ solid solution [13]. In the present work, $SrLa[Al_{1-x}(Mg_{0.5}Ti_{0.5})_x]O_4$ (x = 0.2–0.8) solid solution ceramics were prepared, and the structural evaluation and microwave dielectric properties were investigated.

2. Experimental procedure

$SrLa[Al_{1-x}(Mg_{0.5}Ti_{0.5})_x]O_4$ (x = 0.2, 0.4, 0.6, 0.65, 0.8) ceramics were prepared by a standard solid state sintering method. High-purity $SrCO_3$ (99.95%), La_2O_3 (99.99%), Al_2O_3 (99.99%), MgO (99.9%) and

* Corresponding author.
E-mail address: zjulilei@zju.edu.cn (L. Li).
[1] These authors contribute equally to this work and should be considered as co-first authors.

http://dx.doi.org/10.1016/j.ceramint.2017.10.142
Received 28 August 2017; Received in revised form 19 October 2017; Accepted 21 October 2017

TiO_2 (99.9%) powders were used as raw materials. The raw powders were weighed according to the mole ratio and mixed by ball milling with zirconia media in ethanol for 24 h. After drying, the mixture was calcined at 1350 °C for x = 0.2 and 1400 °C for x = 0.4–0.8 in air for 3 h, and then ball-milled and dried again. The dried powders were mixed with 6 wt% water solution of polyvinyl alcohol (PVA), and pressed into disks of 12 mm in diameter and 2–6 mm in height. These disks were sintered at 1450–1625 °C in air for 3 h to obtain the dense ceramics.

The bulk density of the sintered ceramics was measured by the Archimedes' method. The microstructure on the thermally etched surfaces was observed by a scanning electron microscopy (S-4800, Hitachi, Tokyo, Japan). The phase constitution and crystal structure were identified by powder X-ray diffraction (XRD) analysis with Cu Kα radiation (Rigaku D/max 2550/PC, Rigaku Co., Tokyo, Japan). The XRD data were collected in the 2θ range of 8–130° with a step size of 0.02° and dwelling time of 1.5 s for each step. The structure refinement was conducted by the Rietveld refinement using the FULLPROF program [14].

The ceramics were polished to the roughness of about 1.5 μm for Raman spectrum measurement, which was conducted using an HR-800 LabRaman (Jobin Yvon, Longjumeau, France) at room temperature. The Raman spectrometer was equipped with a Peltier-cooled charge-coupled device and integral Raman microscope. As the excitation source, the 514.532 nm line of an Ar^+ ion laser with an output of 20 mV was adopted. Besides, an Olympus BX4 (Olympus, Tokyo, Japan) microscope with ×50 objective was used for micro-Raman detection. The accumulation times were two collections of 30 s and the range of data was 100–1000 cm^{-1} with the spectral resolution of 1–2 cm^{-1}.

The cylindrical samples of about 10 mm in diameter and 5 mm in thickness were used to evaluate the microwave dielectric properties using a vector network analyzer (E8363B, Agilent Technologies Inc., Palo Alto, CA, USA). The dielectric constant (ε_r) and temperature coefficient of resonant frequency (τ_f) between 20 and 80 °C were measured by the Hakki-Coleman method [15], and the *Qf* value was evaluated by the resonant cavity method [16].

3. Results and discussion

Fig. 1 shows the relative density of $SrLa[Al_{1-x}(Mg_{0.5}Ti_{0.5})_x]O_4$ (x = 0.2, 0.4, 0.6, 0.65, 0.8) ceramics as a function of sintering temperature. The relative density reaches the maximum value over 97% for all the compositions when the sintering temperature is between 1575 and 1625 °C. The high relative density is also confirmed by the SEM images of the ceramics sintered at the optimal temperatures, as shown in Fig. 2, where the dense and uniform microstructure is observed. Besides, the grain size increases significantly with increasing x, which is consistent

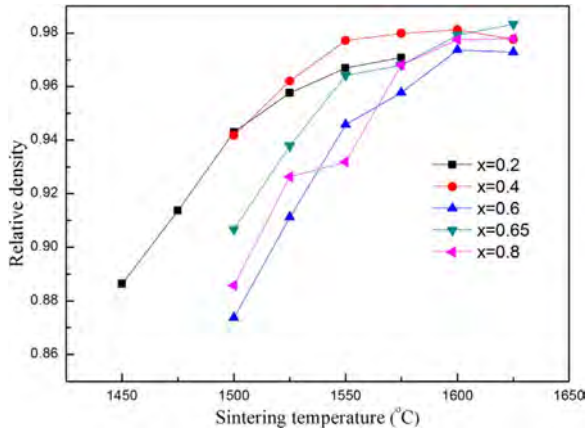

Fig. 1. Relative density of $SrLa[Al_{1-x}(Mg_{0.5}Ti_{0.5})_x]O_4$ (x = 0.2–0.8) ceramics as a function of sintering temperature.

with the results for the end-members $SrLaAlO_4$ [3] and $SrLa(Mg_{0.5}Ti_{0.5})O_4$ [12].

The XRD patterns of $SrLa[Al_{1-x}(Mg_{0.5}Ti_{0.5})_x]O_4$ ceramics sintered at the optimal temperature are shown in Fig. 3(a). All the diffraction peaks can be assigned to those of $SrLaAlO_4$ (JCPDS card No. 24-1125), and the crystallographic planes are indexed. No apparent peaks corresponding to secondary phases are observed, indicating that $SrLaAlO_4$ and $SrLa(Mg_{0.5}Ti_{0.5})O_4$ can form unlimited solid solution, and this is consistent with the prediction in Ref. [12]. Besides, no diffraction peak for superlattice is observed for all the compositions, indicating the absence of cation ordering of Al^{3+}, Mg^{2+} and Ti^{4+} cations at *B* site.

Rietveld refinement has been carried out to further analyze the refined crystal structure of $SrLa[Al_{1-x}(Mg_{0.5}Ti_{0.5})_x]O_4$ ceramics, and Fig. 3(b) shows an example of the experimental and calculated diffraction profiles for x = 0.65. All the diffraction patterns can be successfully indexed as the tetragonal K_2NiF_4–type structure with *I4/mmm* space group, and the refined structural parameters, reliability factors, selected bond lengths and tolerance factor of perovskite layer (*t*) are listed in Table 1, where the definition for the different O atoms and the tolerance factor can be observed in Fig. 3(c) and Ref. [2], respectively. Fig. 4 shows the lattice parameters of $SrLa[Al_{1-x}(Mg_{0.5}Ti_{0.5})_x]O_4$ (x = 0–1) ceramics as functions of x and the effective ionic radius of $[Al_{1-x}(Mg_{0.5}Ti_{0.5})_x]^{3+}$ at *B* site ($r(B^{3+})$) [17], where the data for the end-members $SrLaAlO_4$ and $SrLa(Mg_{0.5}Ti_{0.5})O_4$ are cited from Refs. [3] and [12], respectively. With increasing x and $r(B^{3+})$, the lattice parameter *a* increases near linearly, while *c* first increases to the maximum value at x = 0.65, and then decreases. Besides, *a* increases by 3.44% with increasing x from 0 to 1, while the largest variation of *c* is only 0.32%. In fact, the ions at *A* site usually play a role in the lattice parameter *c* in K_2NiF_4–type structure, while those at *B* site dominates *a* [18]. The ions at *A* site (Sr^{2+}/La^{3+} with the mole ratio of 1:1) are constant in the present solid solutions, so the increase in $r(B^{3+})$ with x leads to a significant increase in *a*, but only a slight change in *c*. As a result, the change in *a* dominate *c/a* and the cell volume, and both of them change near linearly with x and $r(B^{3+})$. Furthermore, the tolerance factor of perovskite layer derives more from 1 with increasing x and $r(B^{3+})$, indicating the decrease in the stability of K_2NiF_4–type structure.

Fig. 5 shows the bond lengths and normalized bond lengths for $SrLa[Al_{1-x}(Mg_{0.5}Ti_{0.5})_x]O_4$ (x = 0–1) ceramics as functions of x and $r(B^{3+})$ [17], where the data for the end-members $SrLaAlO_4$ and $SrLa(Mg_{0.5}Ti_{0.5})O_4$ are cited from Refs. [3] and [12], respectively. Here, the normalized bond length is defined as the actual bond length over the ideal bond length. The ions at *A* site are constant (Sr^{2+}/La^{3+} with the mole ratio of 1:1) in the present solid solutions, so the tendencies for the bond lengths and normalized bond lengths of (Sr/La)-O(1), (Sr/La)-O(2a) and (Sr/La)-O(2b) bonds are the same. In comparison, the effective ion radius of $[Al_{1-x}(Mg_{0.5}Ti_{0.5})_x]^{3+}$ at *B* site depends on the x value, resulting in the different variations for the bond lengths and normalized bond lengths of $[Al/(Mg_{0.5}Ti_{0.5})]$-O(1) and $[Al/(Mg_{0.5}Ti_{0.5})]$-O(2) bonds. As shown in Fig. 5(a), the increases in x and $r(B^{3+})$ lead to the near-linear increase in the bond length of $[Al/(Mg_{0.5}Ti_{0.5})]$-O(1) in *ab* plane, and this is consistent with the lattice parameter *a* (see Fig. 4(a)). Similarly, the bond lengths of (Sr/La)-O(2a) and (Sr/La)-O(1) also increase near linearly with x and $r(B^{3+})$, although they do not lie in, but project on *ab* plane [12]. In comparison, the bond lengths of (Sr/La)-O (2b) and $[Al/(Mg_{0.5}Ti_{0.5})]$-O(2) along *c* axis exhibit opposite variations with x and $r(B^{3+})$, since the lattice parameter *c* is mainly determined by the bond lengths of (Sr/La)-O(2b) and $[Al/(Mg_{0.5}Ti_{0.5})]$-O(2), and it is not sensitive to $r(B^{3+})$ (see Fig. 4(b)). The normalized bond length shown in Fig. 5(b) can be used to evaluate the compression/dilation degree of each bond. When the normalized bond length is over 1, the bond is elongated, otherwise it is compressed. Therefore, (Sr/La)-O(2a) and $[Al/(Mg_{0.5}Ti_{0.5})]$-O(2) bonds are elongated, while (Sr/La)-O(1), (Sr/La)-O(2b) and $[Al/(Mg_{0.5}Ti_{0.5})]$-O(1) bonds are compressed in the present solid solutions. With increasing x, the normalized bond lengths

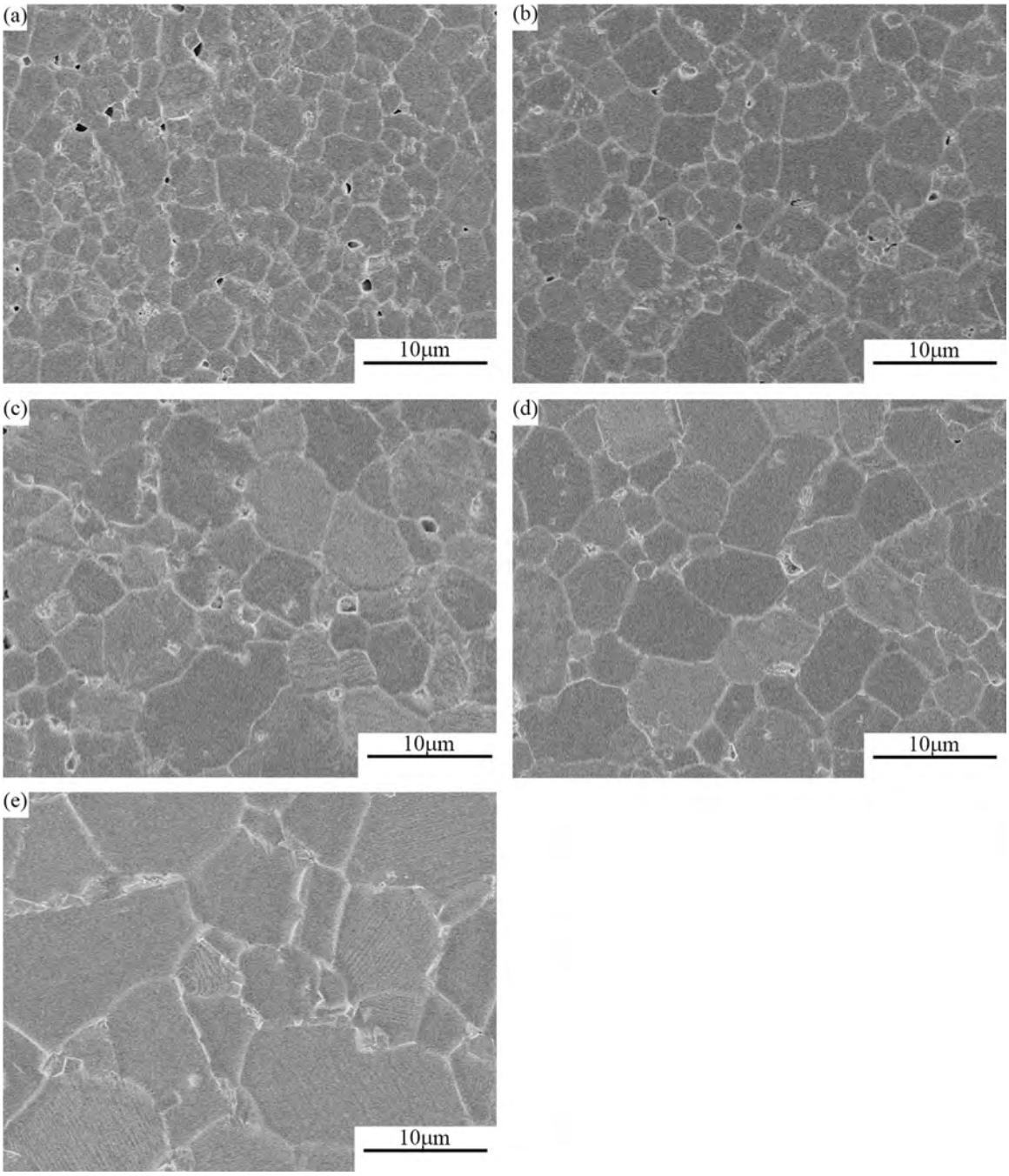

Fig. 2. SEM images on thermally-etched surfaces of $SrLa[Al_{1-x}(Mg_{0.5}Ti_{0.5})_x]O_4$ (x = 0.2–0.8) ceramics sintered at optimum temperatures: (a) x = 0.2, (b) x = 0.4, (c) x = 0.6, (d) x = 0.65, and (e) x = 0.8.

of (Sr/La)-O(1) and (Sr/La)-O(2a) increases near linearly, indicating that the former is more elongated, and the latter is less compressed. The reverse trend is observed for $[Al/(Mg_{0.5}Ti_{0.5})]$-O(1) bond, which becomes more compressed with increasing x. The normalized bond lengths of (Sr/La)-O(2b) and $[Al/(Mg_{0.5}Ti_{0.5})]$-O(2) exhibit non-monotonous variations with x. The (Sr/La)-O(2b) bond first becomes less compressed with increasing x from 0 to 0.2, and it becomes more compressed with further increasing x. In comparison, the $[Al/(Mg_{0.5}Ti_{0.5})]$-O(2) bond first becomes less elongated with increasing x from 0 to 0.2, and the elongation degree does not change much with further increasing x. The variations of the normalized bond lengths play a role in the dielectric constant of the present solid solutions, which will be discussed in the last paragraph.

Fig. 6(a) shows the Raman spectra of $SrLa[Al_{1-x}(Mg_{0.5}Ti_{0.5})_x]O_4$ (x = 0–1) ceramics, where six groups of bands are observed and labeled. According to the factor group analysis, there are four Raman-active modes with two A_{1g} and two E_g symmetries for K_2NiF_4–type structure with *I*4/mmm space group [19]. Band 1 with the lowest Raman shift is assigned to the vibration of the (Sr/La)-O(2a) bond in the *ab* plane in E_g symmetry [20,21]. It is very weak and cannot be observed for x = 0–0.2. Bands 2 and 3 are assigned to the vibrations of the (Sr/La)-O(2b) bond along *c* axis in A_{1g} symmetry and the bridge (Sr/La)-O(2a)-(Sr/La) oxygen bond in E_g symmetry, respectively [20,21], and both of them become weaker with increasing x. Band 4 corresponds to the vibration of the bridge (Sr/La)-O(2b)-$[Al/(Mg_{0.5}Ti_{0.5})]$ oxygen bond along *c* axis in A_{1g} symmetry [20,21]. Bands 5 and 6 are not predicted by the factor group analysis. Band 5 has been reported in many K_2NiF_4–type compounds, and its origin remains under debate. As suggested by Heyen

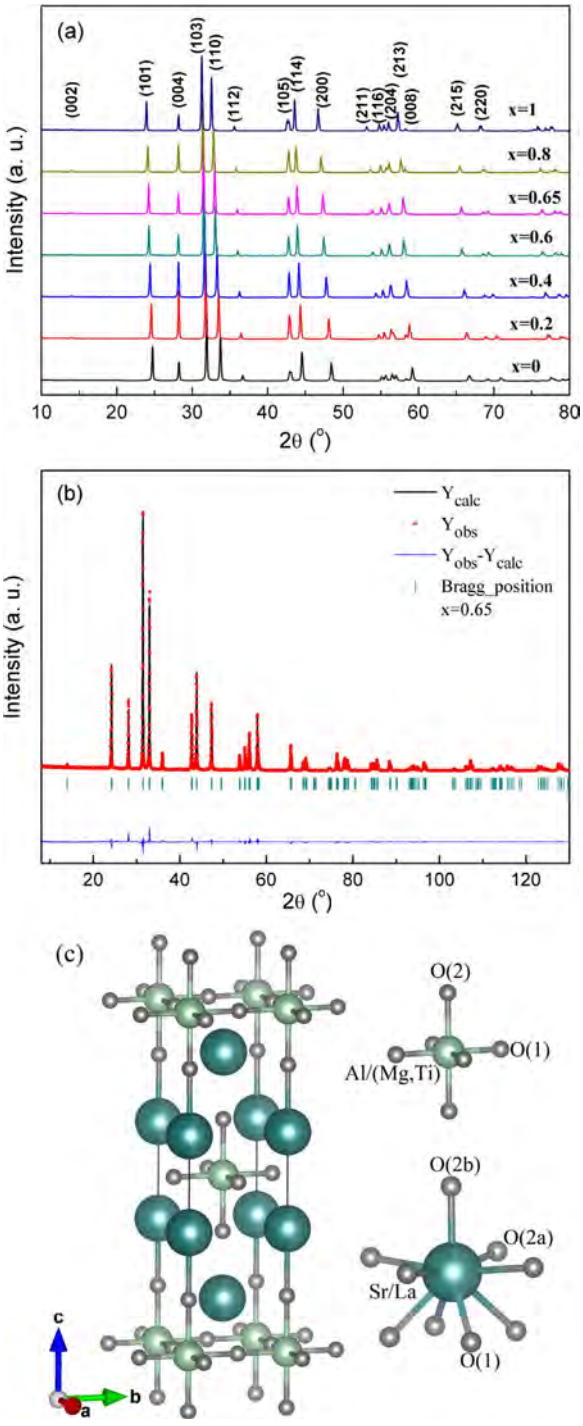

Fig. 3. (a) XRD patterns of $SrLa[Al_{1-x}(Mg_{0.5}Ti_{0.5})_x]O_4$ (x = 0–1) ceramics sintered at optimum temperatures. (b) Experimental (circles) and calculated (black line) XRD profiles for x = 0.65. The short vertical lines below the pattern mark the positions of Bragg reflections. The bottom continuous line shows the difference between the experimental and calculated intensities. (c) Crystal structure of $SrLa[Al_{1-x}(Mg_{0.5}Ti_{0.5})_x]O_4$ (x = 0–1).

et al., bond 5 corresponds to an in-plane $[Al/(Mg_{0.5}Ti_{0.5})]$-O stretching [22], while Margez et al. argued that it may be induced by defects [21]. Both bands 4 and 5 are split into two bands for high x value, and it should be related to the large difference between Mg^{2+} and Ti^{4+} at *B* site. The strong band 6 is observed with the highest Raman shift except for x = 0. In fact, this band has been reported in the K_2NiF_4–type compounds with Ti^{4+} [13,23] or Mg^{2+} [20] at *B* site, while it is absent for those with only Al^{3+} at *B* site [13,23]. Therefore, band 6 is regarded to be attributed to the vibration of $(Mg_{0.5}Ti_{0.5})$-O(2) bond along *c* axis in A_{1g} symmetry [13,23].

The Raman shift of the above bands as a function of x is shown in Fig. 6(b), where bands 1 and 5 are absent since they are too weak. The Raman shift for bands 3 and 4 decreases near linearly with increasing x. As discussed above, band 3 is assigned to the vibration of the bridge (Sr/La)-O(2a)-(Sr/La) oxygen bond. The increasing normalized bond length of (Sr/La)-O(2a) with x (see Fig. 5(b)) corresponds to the decrease in the bond strength, and thus leads to the decreasing Raman shift. Band 4 corresponds to the bridge (Sr/La)-O(2b)-$[Al/(Mg_{0.5}Ti_{0.5})]$ oxygen bond, and the different variations of the normalized bond lengths of (Sr/La)-O(2b) and $[Al/(Mg_{0.5}Ti_{0.5})]$-O(2) shown in Fig. 5(b) have opposite effects on the Raman shift. It is indicated that the significant increase in the mole mass of $[Al_{1-x}(Mg_{0.5}Ti_{0.5})_x]^{3+}$ with x dominates the decreasing Raman shift of this band. The Raman shift of band 6 that corresponds to the $(Mg_{0.5}Ti_{0.5})$-O(2) bond first decreases slowly with increasing x from 0.2 to 0.65, and then decreases more rapidly with further increasing x. Similar results have been reported in $SrLa[Al_{1-x}(Zn_{0.5}Ti_{0.5})_x]O_4$ solid solutions [13]. Since the normalized bond length of $[Al/(Mg_{0.5}Ti_{0.5})]$-O(2) does not change much for x = 0.2–1 (see Fig. 5(b)), the increasing mole mass of $(Mg_{0.5}Ti_{0.5})_x$ with x should be responsible for the decrease in the Raman shift. Furthermore, a contradiction is observed for band 2, which corresponds to (Sr/La)-O (2b) bond. According to the normalized bond length of (Sr/La)-O(2b) in Fig. 5(b), the Raman shift of band 2 should first decreases and then increases with x. However, the measured Raman shift first increases, and then decreases, as shown in Fig. 6(b). The reason for this contradiction remains unclear.

The microwave dielectric properties of $SrLa[Al_{1-x}(Mg_{0.5}Ti_{0.5})_x]O_4$ ceramics are shown in Fig. 7. With increasing x from 0 to 1, the dielectric constant increases monotonously from 17.6 to 25.5, while the *Qf* value first increases slightly, and then decreases gradually. Since $SrLaAlO_4$ and $SrLa(Mg_{0.5}Ti_{0.5})_xO_4$ can form unlimited solid solution, and no structural phase transition is observed in their solid solutions, the temperature coefficient of resonant frequency increases with ε_r and x. The end-members $SrLaAlO_4$ and $SrLa(Mg_{0.5}Ti_{0.5})O_4$ are of negative and positive τ_f values, respectively, so near-zero τ_f value can be achieved in the solid solutions. Thus, the optimal microwave dielectric properties with ε_r = 22.2, *Qf* = 89,100 GHz and τ_f = −0.1 ppm/°C are obtained for x = 0.65, indicating that the present ceramic is a promising candidate as low-loss microwave dielectric materials.

The significant increase in ε_r with x is an interesting issue that is worthy to be further investigated. It is well known that the dielectric constant of a solid can be predicted from the molecule polarizability α_D based on the Clausius-Mosotti relation

$$\frac{\varepsilon_r-1}{\varepsilon_r+2}=\frac{4\pi\alpha_D}{3V_m}, \quad (1)$$

where the mole volume V_m is half of the unit cell volume of the compounds with K_2NiF_4–type structure, and α_D can be calculated as the sum of the constituting ionic polarizabilities. The effective ionic polarizability of $(Mg_{0.5}Ti_{0.5})^{3+}$ (2.135 Å^3) is higher than Al^{3+} (0.78 Å^3) [24], and may be responsible for the increase in ε_r with x. However, considering the ionic polarizabilities of Sr^{2+} (4.25 Å^3), La^{3+} (6.03 Å^3) and O^{2-} (2.00 Å^3) [24], α_D only increases from 19.06 to 20.415 Å^3 with increasing x from 0 to 1, and the increase in α_D is not large enough to explain the rapid increase in ε_r. Besides, V_m increases from 178.4 to 191.8 Å^3 with increasing x from 0 to 1 (see Fig. 4(d)), which has an opposite effect on ε_r. As the result of the above two factors, the predicted dielectric constant from Eq. (1) decreases slightly with increasing x, although the measured value increases significantly (see Fig. 8(a)). This contradiction can be explained by the variations of the normalized bond lengths of (Sr/La)-O bonds. According to Ref. [2], the contribution of the $E_u(1)$ and $A_{2u}(1)$ lattice vibration modes to the dielectric constant of $SrLnAlO_4$ (Ln = La, Nd, Sm) is 72–76% of the total contribution of all infrared-active modes, and therefore play a role in the final dielectric constant. The two modes correspond to the ionic vibrations of (Sr/La)

Table 1
Structural parameters, reliability factors, and bond lengths of $SrLa[Al_{1-x}(Mg_{0.5}Ti_{0.5})_x]O_4$ ceramics.

	x = 0.2	x = 0.4	x = 0.6	x = 0.65	x = 0.8
a (Å)	3.78247(4)	3.80713(4)	3.83366(4)	3.84072(3)	3.86156(4)
c (Å)	12.65619(1)	12.66969(1)	12.67563(1)	12.67638(1)	12.67198(1)
c/a	3.3460	3.3279	3.3064	3.3005	3.2816
V_{cell} (Å^3)	181.0731	183.6375	186.2931	186.9909	188.9601
$(Sr, La)_z$ (Å)	0.35872(4)	0.35885(4)	0.35931(4)	0.35898(4)	0.35876(4)
$O(2)_z$ (Å)	0.1614(3)	0.1632(2)	0.1657(3)	0.1659(3)	0.1677(3)
R_p	6.00	5.17	3.61	5.81	5.73
R_{wp}	7.58	6.87	7.43	7.43	7.49
R_B	3.36	3.39	5.84	3.62	3.62
χ^2	5.09	4.11	4.24	4.21	4.27
$Al/(Mg_{0.5}Ti_{0.5})$-O(1) (Å)	1.8912(35)	1.9035(65)	1.9168(30)	1.9203(60)	1.9307(80)
$Al/(Mg_{0.5}Ti_{0.5})$-O(2) (Å)	2.043(4)	2.068(3)	2.100(4)	2.103(4)	2.125(4)
Sr/La-O(1) (Å)	2.6027(3)	2.6118(3)	2.6181(3)	2.6236(3)	2.6327(3)
Sr/La-O(2a) (Å)	2.6867(4)	2.7065(3)	2.7293(4)	2.7341(4)	2.7510(5)
Sr/La-O(2b) (Å)	2.497(4)	2.479(3)	2.454(4)	2.448(4)	2.421(4)
t	0.96048	0.94815	0.93613	0.93317	0.92441

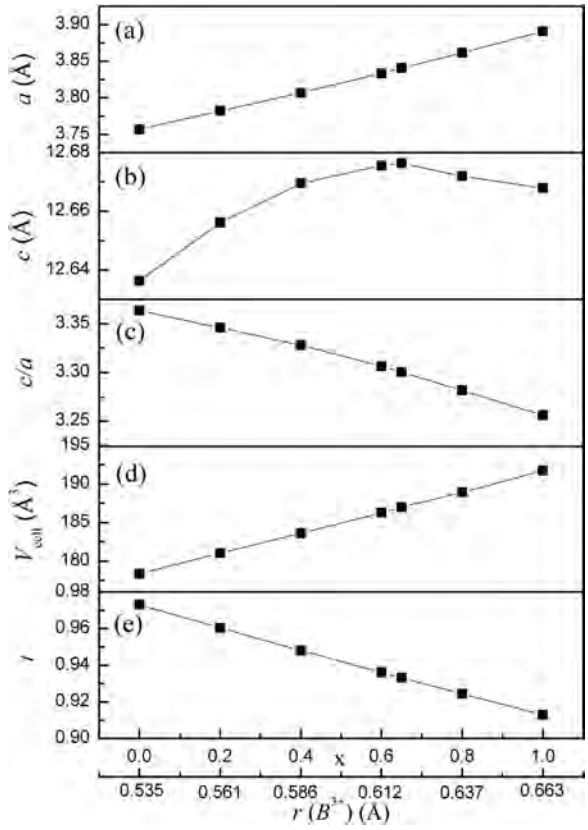

Fig. 4. Structural parameters of $SrLa[Al_{1-x}(Mg_{0.5}Ti_{0.5})_x]O_4$ (x = 0–1) ceramics as functions of x and $r(B^{3+})$: (a) a, (b) c, (c) c/a, (d) cell volume and (e) tolerance factor of perovskite layer.

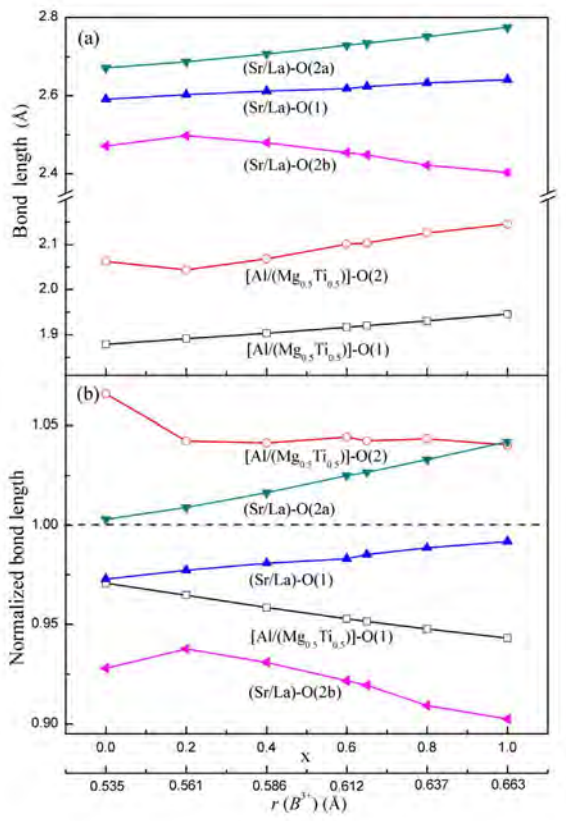

Fig. 5. (a) Bond lengths and (b) normalized bond lengths for $SrLa[Al_{1-x}(Mg_{0.5}Ti_{0.5})_x]O_4$ (x = 0–1) ceramics as functions of x and $r(B^{3+})$.

O_9 dodecahedron in *ab* plane and along *c* axis, respectively for the present ceramics. As shown in Fig. 5(b), Sr/La-O(2a) bond is only slightly elongated for $SrLaAlO_4$, while Sr/La-O(1) and Sr/La-O(2b) bonds are heavily compressed. Therefore, the contribution of these two modes to dielectric constant is strongly suppressed for x = 0, so that the difference between the measured and predicted dielectric constants ($\Delta\varepsilon_r$) is a large negative value (see Fig. 8(b)). With increasing x, both the normalized bond lengths of Sr/La-O(1) and Sr/La-O(2a) increases significantly, indicating that the contribution of $E_u(1)$ and $A_{2u}(1)$ modes to dielectric constant is greatly enhanced. Although Sr/La-O(2b) bond may become more compressed, there are four equivalent O(1) atoms, four equivalent O(2a) atoms, while only one O(2b) atom in a Sr/La-centered dodecahedron. This means that the effect of the Sr/La-O(2b) bond is much weaker than those of Sr/La-O(1) and Sr/La-O(2a) bonds. As a result, therefore, the contribution of the $E_u(1)$ and $A_{2u}(1)$ lattice vibration modes to the dielectric constant are enhanced significantly with increasing x, and $\Delta\varepsilon_r$ increases from a large negative value for x = 0 and approaches 0 for x = 1.

4. Conclusion

The dense $SrLa[Al_{1-x}(Mg_{0.5}Ti_{0.5})_x]O_4$ (x = 0.2–0.8) solid solution ceramics with K_2NiF_4–type layered perovskite structure and *I4/mmm* space group were prepared by a standard solid state reaction method, and the structural evaluation was investigated by Rietveld analysis of XRD and Raman spectrum. With increasing x, the dielectric constant

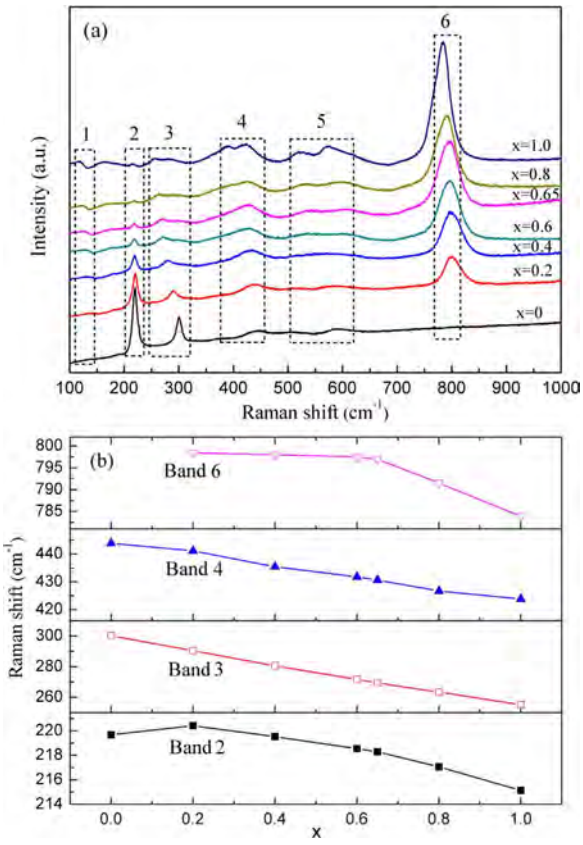

Fig. 6. (a) Raman spectra of $SrLa[Al_{1-x}(Mg_{0.5}Ti_{0.5})_x]O_4$ ceramics, and (b) Raman shift of bands 2, 3, 4 and 6 as a function of x.

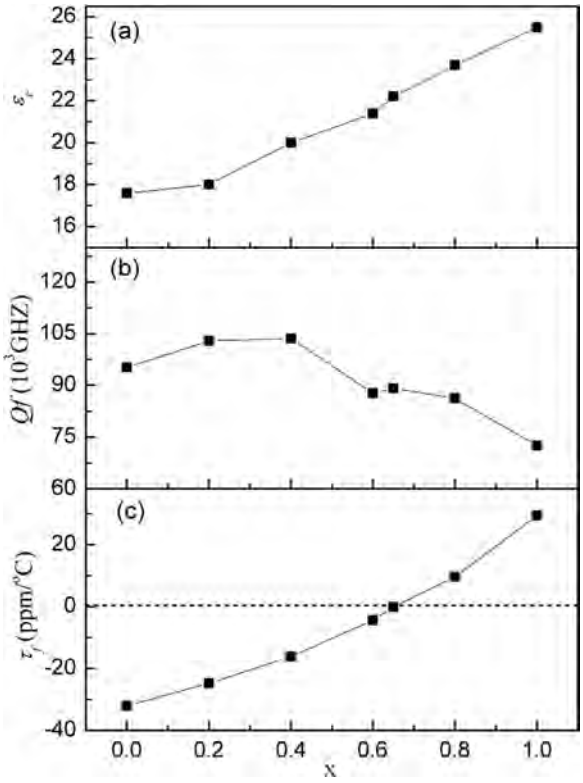

Fig. 7. (a) Dielectric constant, (b) *Qf* value and (c) temperature coefficient of resonant frequency of $SrLa[Al_{1-x}(Mg_{0.5}Ti_{0.5})_x]O_4$ ceramics as functions of x.

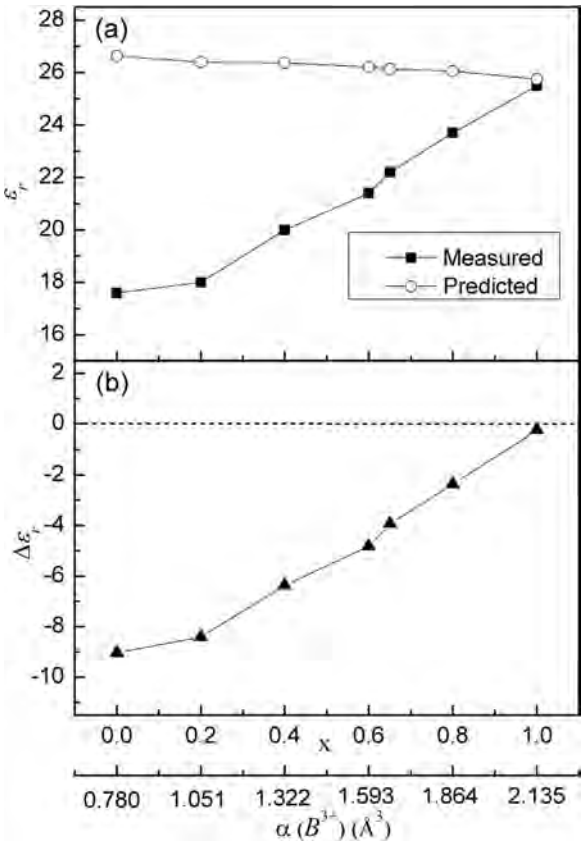

Fig. 8. (a) Measured and predicted dielectric constants, and (b) difference between measured and predicted dielectric constants of $SrLa[Al_{1-x}(Mg_{0.5}Ti_{0.5})_x]O_4$ ceramics as functions of x and $\alpha(B^{3+})$.

and temperature coefficient of resonant frequency increased, while the *Qf* value first increased and then decreased. The difference between the measured and predicted dielectric constants was a large negative value for x = 0, and its absolute value decreased with increasing x, which is mainly attributed to the increasing normalized bond lengths of Sr/La-O (1) and Sr/La-O(2a) bonds. The optimal microwave dielectric properties with ε_r = 22.2, *Qf* = 89,100 GHz and τ_f = −0.1 ppm/°C were obtained for x = 0.65, indicating that $SrLa[Al_{1-x}(Mg_{0.5}Ti_{0.5})_x]O_4$ solid solution is a promising candidate as low-loss microwave dielectric ceramics.

Acknowledgments

This work was financially supported by National Key Research and Development Program of China under Grant No. 2017YFB0406301 and Science and Technology Program of Zhejiang Province under Grant No. 2016C31006.

References

[1] Y. Xiao, X.M. Chen, X.Q. Liu, Microstructures and microwave dielectric characteristics of $CaReAlO_4$ (Re = Nd, Sm and Y) ceramics with tetragonal K_2NiF_4 structure, J. Am. Ceram. Soc. 87 (2004) 2143–2146.

[2] X.C. Fan, X.M. Chen, X.Q. Liu, Structural dependence of microwave dielectric properties of $SrRAlO_4$ (*R* = Sm, Nd, La) ceramics: crystal structure refinement and infrared reflectivity study, Chem. Mater. 20 (2008) 4092–4098.

[3] M.M. Mao, X.M. Chen, X.Q. Liu, Structure and microwave dielectric properties of solid solution in $SrLaAlO_4$-Sr_2TiO_4 system, J. Am. Ceram. Soc. 94 (2011) 3948–3952.

[4] H.X. Yuan, X.M. Chen, M.M. Mao, Structure and microwave dielectric characteristics of $Ca_{1+x}Nd_{1-x}Al_{1-x}Ti_xO_4$ ceramics, J. Am. Ceram. Soc. 92 (2009) 2286–2290.

[5] M.M. Mao, X.C. Fan, X.M. Chen, Effect of A-site ionic radius on the structure and microwave dielectric characteristics of $Sr_{1+x}Sm_{1-x}Al_{1-x}Ti_xO_4$ ceramics, Int. J.

Appl. Ceram. Technol. 7 (2010) E156–E162.
[6] C. Zhang, L. Yi, L. Li, X.M. Chen, Structure and microwave dielectric characteristics of solid solutions in $SrNdAlO_4$-Sr_2TiO_4 system, Int. J. Appl. Ceram. Technol. (2013) 1–7.
[7] Y. Higuchi, H. Tamura, Recent progress on the dielectric properties of dielectric resonator materials with their applications from microwave to optical frequencies, J. Eur. Ceram. Soc. 23 (2003) 2683–2688.
[8] N. Ichinose, T. Shimada, Effect of grain size and secondary phase on microwave dielectric properties of $Ba(Mg_{1/3}Ta_{2/3})O_3$ and $Ba([Mg,Zn]_{1/3}Ta_{2/3})O_3$ systems, J. Eur. Ceram. Soc. 26 (2006) 1755–1759.
[9] F. Lichtenberg, A. Herrnberger, K. Wiedenmann, Synthesis, structural, magnetic and transport properties of layered perovskite-related titanates, niobates and tantalates of the type $A_nB_nO_{3n+2}$, $A'A_{k-1}B_kO_{3k+1}$ and $A_mB_{m-1}O_{3m}$, Prog. Solid. State Chem. 36 (2008) 253–387.
[10] S.Y. Cho, C.H. Kim, D.W. Kim, K.S. Hongs, Dielectric properties of $Ln(Mg_{1/2}Ti_{1/2})O_3$ as substrates for high Tc superconducting thin films, J. Mater. Res. 14 (1999) 2484–2487.
[11] R. Ubic, Y. Hu, K. Khamoushi, I. Abrahams, Structure and properties of $La(Zn_{1/2}Ti_{1/2})O_3$, J. Eur. Ceram. Soc. 26 (2006) 1787–1790.
[12] G.R. Ren, J.Y. Zhu, L. Li, B. Liu, X.M. Chen, $SrLa(R_{0.5}Ti_{0.5})O_4$ (R = Mg, Zn) microwave dielectric ceramics with complex K_2NiF_4-type layered perovskite structure, J. Am. Ceram. Soc. 100 (2017) 2582–2589.
[13] B. Liu, L. Li, X.Q. Liu, X.M. Chen, Structural evolution of $SrLaAl_{1-x}(Zn_{0.5}Ti_{0.5})_xO_4$ ceramics and effects on their microwave dielectric Properties, J. Mater. Chem. C 4 (2016) 4684–4691.
[14] J. Rodriguez-Carvajal, Recent developments of the program FULLPROF in commission on powder diffraction, Int. Union Crystallogr. Newsl. 26 (2001) 12–19.
[15] B.W. Hakki, P.D. Coleman, A dielectric resonant method of measuring inductive capacitance in the millimeter range, IEEE Trans. Microw. Theory Tech. 8 (1960) 402–410.
[16] X.C. Fan, X.M. Chen, X.Q. Liu, Complex-permittivity measurement on high-Q materials via combined numerical approaches, IEEE Trans. Microw. Theory Tech. 53 (2005) 3130–3134.
[17] R.D. Shannon, Revised effective ionic radii and systematic studies of interatomic distances in halides and chalcogenides, Acta Crystallogr. A32 (1976) 751–767.
[18] A.E. Lavat, E.J. Baran, IR-Spectroscopic behaviour of $AA'BO_4$ oxides belonging to the K_2NiF_4 structural type, J. Alloy. Compd. 368 (2004) 130–134.
[19] D.L. Rousseau, R.P. Bauman, S.P.S. Porto, Normal mode determination in crystals, J. Raman Spectrosc. 10 (1981) 253–290.
[20] A. Magrez, M. Cochet, O. Joubert, G. Louarn, M. Ganne, O. Chauvet, High internal stresses in $Sr_{1-x}La_{1+x}Al_{1-x}Mg_xO_4$ solid solution ($0 \le x \le 0.7$) characterized by infrared and raman spectroscopies coupled with crystal structure refinement, Chem. Mater. 13 (2001) 3893–3898.
[21] V.G. Hadjiev, M. Cardonaa, I. Ivanovb, V. Popovb, M. Gyulmezovb, M.N. Ilievb, M. Berkowski, Optical phonons probe of the $SrLaAlO_4$ crystal structure, J. Alloy. Compd. 251 (1997) 7–10.
[22] E.T. Heyen, R. Liu, M. Cardona, S. Pinol, R.J. Melville, D. Mc.K. Paul, Phonon anomalies and structural stability in the $R_{2-x}Ce_xCuO_4$ system (R = Gd, Sm, Nd, Pr) Optical phonons probe of the $SrLaAlO_4$ crystal structure, Phys. Rev. B 43 (1991) 2857–2865.
[23] M.M. Mao, X.Q. Liu, X.M. Chen, Structural evolution and its effects on dielectric loss in $Sr_{1+x}Sm_{1-x}Al_{1-x}Ti_xO_4$ microwave dielectric ceramics, J. Am. Ceram. Soc. 94 (2011) 2506–2511.
[24] R.D. Shannon, Dielectric polarizabilities of ions in oxides and fluorides, J. Appl. Phys. 73 (1993) 348–366.